

Proposal of Guidelines for Reducing Iron loss of Soft Magnetic Composite Cores by Quantitative Analysis of Factors Affecting Coercive Field

TAKASHITA Takuya*¹ HIRATANI Tatsuhiko*² NAKAMURA Naomichi*³

Abstract:

A proposal of guidelines for reducing the iron loss of soft magnetic composite (SMC) cores was studied by a quantitative analysis of hysteresis loss-related microstructural factors with the aim of expanding the application of SMC cores. Analysis of the iron loss of SMC cores by a quantitative analysis model revealed that crystal grain coarsening is an effective approach for reducing iron loss. The iron loss of a SMC core (iron powder particle size: 75 μm) with $B = 1.0$ T, $f = 1$ kHz when the crystal grains were coarsened to the maximum possible extent was calculated by the analysis model, and the loss was the same as that of an electrical steel with a thickness of 0.2 mm.

1. Introduction

As features of SMC cores produced by compaction of insulation-coated soft magnetic powder such as iron powder, the following three points are generally mentioned:

- ① Higher saturation magnetization compared with oxide sintered magnetic cores such as ferrite cores.
- ② Lower eddy current loss compared with laminated cores such as electrical steel sheet cores.
- ③ Three-dimensionally isotropic magnetic properties and ease of obtaining near-net shapes.

Some previous studies have suggested that reactors and inductors are suitable applications of SMC core because of features ① and ②¹⁾, and in recent years, application of an axial gap motor using a SMC core has been reported, taking advantage of feature ③²⁾.

While examples of the above applications are increasing, SMC also has some problems in terms of magnetic properties, including higher hysteresis loss

compared with electrical steel sheets. Iron loss is generally expressed by the sum of hysteresis loss W_h and eddy current loss W_e , as shown in the following equation.

$$W = W_h + W_e \dots\dots\dots (1)$$

Where W_h is proportional to the excitation frequency, and W_e is proportional to the square of the excitation frequency³⁾. In applications with low excitation frequencies below 1 kHz, such as motor cores, the effect of hysteresis loss on iron loss is larger than that of eddy current loss. Since the hysteresis loss of SMC cores is higher than that of electrical steel⁴⁾, decreased motor efficiency due to application of SMC cores to motors is a concern.

Against this background, reduction of the hysteresis loss of SMC cores is important for expanding the application of this type of core, and various studies have been carried out⁵⁻⁶⁾. However, in most cases, quantitative discussion of hysteresis loss was difficult because multiple factors affected the hysteresis loss of the SMC cores in those studies, and it is difficult to separate those factors quantitatively. Thus, to further reduce the hysteresis loss of SMC cores, it is important to quantitatively separate the factors affecting hysteresis loss and reduce the influence of each factor.

Therefore, in this study, the following were carried out to clarify guidelines for reducing the hysteresis loss of SMC cores. First, the conventional knowledge on the microstructural factors that affect coercivity, which is strongly correlated with hysteresis loss, was arranged, and relational equations for hysteresis loss and microstructural factors were derived. Then, the influence of microstructural factors on the hysteresis loss of SMC cores was quantified, and the factor with the greatest

[†] Originally published in *JFE GIHO* No. 52 (Aug. 2023), p. 55–61

^{*2} Dr. Eng., Senior Researcher Manager, Sustainable Materials Research Dept., Steel Res. Lab., JFE Steel

^{*1} Dr. Eng., Senior Researcher Manager, Stainless Steel & Iron Powder Research Dept., Steel Res. Lab., JFE Steel

^{*3} Dr. Eng., Director, JFE Precision

influence on core iron loss was clarified. Finally, guidelines for reducing the iron loss of SMC cores were proposed based on the above findings.

2. Mechanism of Coercivity

2.1 Hysteresis Loss and Coercivity

Takajo⁷⁾ expressed the hysteresis loss of sintered iron cores as shown in Eq. (2)

$$W_h = (4 \cdot c_h \cdot B \cdot f \cdot H_c) / \rho_c \dots \dots \dots (2)$$

Where B is excitation magnetic flux density, f is excitation frequency, ρ_c is core density, c_h is a constant determined by the shape of the hysteresis loop and H_c is coercivity. B and f depend on the evaluation conditions, and ρ_c and c_h depend on the chemical composition of the raw material and the manufacturing conditions of the core. When the factors other than H_c are constants, hysteresis loss is proportional to the coercivity.

A schematic image of the microstructure of a SMC core is shown in Fig. 1. In SMC cores, domain wall pinning sites such as the crystal grain boundary, particle surfaces, pores, dislocations and inclusions are considered as factors that increase coercivity. Although few studies have examined the influence of these factors on the coercivity of SMC cores, some studies on the coercivity of steel sheets and bulk metals have been reported. Therefore, we studied the quantification of the influence of microstructural factors on the coercivity of SMC cores⁸⁻¹¹⁾. The following describes the influence of the crystal grain boundary and dislocations, which have large influences on coercivity.

2.2 Influence of Crystal Grain Boundary

For the influence of the crystal grain boundary on coercivity, Mager¹²⁾, Yensen et al.¹³⁾ and Döring¹⁴⁾ proposed a model proportional to the reciprocal of the crystal grain size. Previous studies on Fe-Ni¹⁵⁾, Fe-Si¹⁶⁾ and Fe-Co¹⁷⁾ have shown that a linear relationship

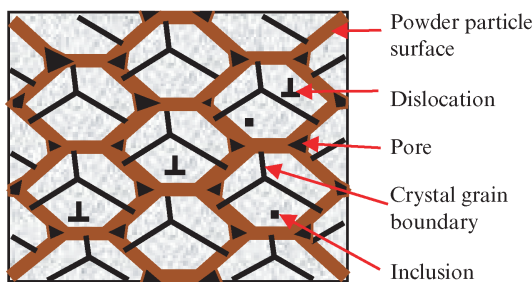


Fig. 1 Schematics of microstructure of SMC (Soft Magnetic Composite) cores

exists between coercivity and the reciprocal of the crystal grain size. The model equation is expressed by Eq. (3)

$$H_{c,k} = (3 \cdot \gamma) / (I_s \cdot d_k) \dots \dots \dots (3)$$

Where $H_{c,k}$ is the contribution of the crystal grain boundary, I_s is saturation magnetization, d_k is the crystal grain size and γ is domain wall energy. Domain wall energy γ is expressed by Eq. (4)¹⁸⁾.

$$\gamma = a (A \cdot K)^{1/2} \dots \dots \dots (4)$$

Where a is a constant determined by the kind of domain wall energy and is 1 for a 90° domain walls and 2 for 180° domain walls, A is a stiffness constant and K is magnetocrystalline anisotropy. By substituting Eq. (4) into Eq. (3), Eq. (5) is obtained.

$$H_{c,k} = (3 \cdot a (A \cdot K)^{1/2}) / (I_s \cdot d_k) \dots \dots \dots (5)$$

For pure iron, I_s , A and K are 2.16 T¹⁹⁾, 1.49·10⁻¹¹ J m⁻¹²⁰⁾ and 4.72·10⁴ J m⁻³²¹⁾, respectively.

In pure iron, the relationship between $H_{c,k}$ and the reciprocal of the crystal grain size is shown in Fig. 2. The grain size dependence of 90° domain wall energy is larger than that of 180° domain wall energy, and the slopes of 90° and 180° domain wall energy are 2.3·10³ and 1.2·10³, respectively. Thus, if the coercivity of pure iron varies due to the crystal grain boundary, the reciprocals of coercivity and the crystal grain size will have a linear relationship, as shown in Fig. 2, and the slope will be within the range of 1.2·10³ to 2.3·10³.

2.3 Influence of Dislocations

Kronmüller et al.²²⁾ studied the influence of dislocations on coercivity in terms of the relationship between the stress field and magnetic moment around dislocations. Träuble²³⁾ then extended the study to the interac-

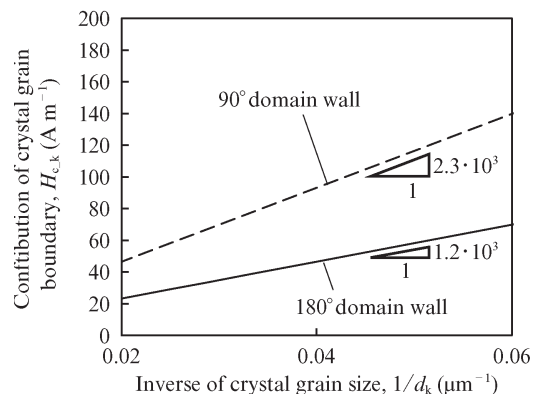


Fig. 2 Relationship between inverse of crystal grain size and $H_{c,k}$

tion of dislocations with domain walls and obtained the following relational equation:

$$H_{c_dis} = \gamma_{dis} \cdot \rho_d^{1/2} \dots\dots\dots (6)$$

Where H_{c_dis} is the contribution of a dislocation, ρ_d is the dislocation density and γ_{dis} is a coefficient determined by magnetostriction and the distribution of domain walls and dislocations. It is difficult to determine γ_{dis} due to the difficulty of quantifying the distribution of domain walls and dislocations. However, if γ_{dis} is assumed to be a constant, coercivity and the square root of ρ_d have a linear relationship. Yaegashi et al.²⁴⁾ studied the relationship between the dislocation density and coercivity in a specimen of pure iron after a tensile test, and reported that the relationship can be explained convincingly by Eq. (6).

2.4 Relationship between Hysteresis Loss and Coercivity Factors

Pfeifer et al.²⁵⁾ proposed an addition rule for the contribution of coercivity, which states that coercivity can be expressed as the sum of the respective contributions of the coercivity factors, and Adler et al.²⁶⁾ showed that the model equation is consistent. In this study, we assume that the addition rule holds for the contributions described in the previous section under the model of Pfeifer et al., and propose the following equation.

$$H_c = H_{c_k} + H_{c_dis} + H_{c_ex} \dots\dots\dots (7)$$

Where H_{c_ex} is the sum of the coercivity factors other than the contributions discussed in this chapter.

A model equation that directly relates hysteresis loss and microstructural factors can be derived by substituting Eq. (7) into Eq. (2).

$$\begin{aligned} W_h &= (4 \cdot \chi_{ch} \cdot B \cdot f) \cdot (H_{c_k} + H_{c_dis} + H_{c_ex}) / \rho_c \\ &= W_{h_k} + W_{h_dis} + W_{h_ex} \dots\dots\dots (8) \end{aligned}$$

Where W_{h_k} is the contribution of the crystal grain boundary, W_{h_dis} is the contribution of dislocations and W_{h_ex} is the contribution of other factors. In the next

chapter, the hysteresis loss of SMC cores is analyzed by using this equation.

3. Analysis of Actual Specimens by Using Model Equation

3.1 Iron Loss and Manufacturing Conditions of SMC Cores

The SMC core manufacturing process is shown in Fig. 3. Several factors affect iron loss in the manufacturing process. The effects of the particle size of the raw iron powder and heat treatment conditions are particularly large, and various studies have attempted to optimize these factor⁵⁻⁶⁾. However, there are few studies on quantitative analysis of the relationship between hysteresis loss and the microstructure factors. In this chapter, SMC cores with different particle sizes and heat treatment conditions were prepared, their hysteresis losses were analyzed by using the model equation derived in the previous chapter, and hysteresis loss reduction guidelines were proposed.

3.2 Experimental Procedure

Four kind of raw iron powders, A-D, which were sieved from water-atomized iron powder, were used. The apparent densities, average particle size d_{p_50} measured by laser diffraction and chemical compositions are shown in Table 1. The apparent densities of pow-

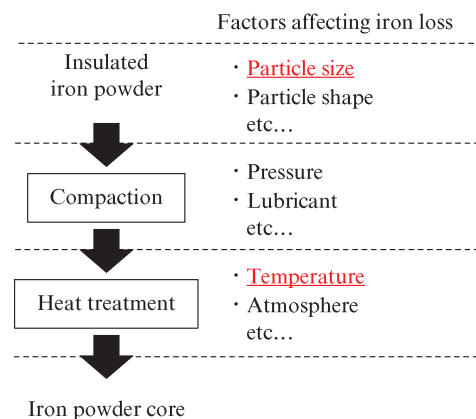


Fig. 3 Production process of SMC cores

Table 1 Powder properties of raw material iron powders

PowderID	Apparent density (Mg m ⁻³)	Average particle size diameter (mm)	Chemical composition (mass%)			
			C	S	O	N
A	3.53	187.3	0.002	0.001	0.032	<0.001
B	3.47	147.9	0.003	0.001	0.027	
C	3.43	107.5	0.002	0.001	0.024	
D	3.50	75.8	0.003	0.001	0.027	

ders A to D were in the range of $3.5 \pm 0.1 \text{ Mg m}^{-3}$, and the impurities (including Al, Si, P, Cr and Mn) of these powders were under 0.01 mass%. The powders were insulated with 0.2 mass% of silicone resin (Dow, SR2400). Next, the insulated powders were compacted into a ring shape (outer diameter: 38 mm, inner diameter: 25 mm, height: 6 mm), and SMC cores A', B', C' and D' were obtained. The densities of these cores were optimized to 7.6 Mg m^{-3} by controlling the compaction pressure. The cores were then heat treated at 873 K with a soaking time of 2.7 ks in a N_2 atmosphere. Core D' was also heat treated at temperatures of 673, 773 and 973 K. The cores heat treated at the different temperatures were identified by adding the symbols -673, -773, -873 and -973 to the letter designation.

The coercive fields and hysteresis losses of all the cores were measured with a DC B-H loop analyzer (Metron Inc., type SK-110). The evaluation was carried out under the conditions of 100 turns of the primary coil, 20 turns of the secondary coil and an excitation magnetic flux density of 1.0 T. Hysteresis loss was calculated by calculating the loss for one period from the area of the DC B-H loop and multiplying the result by the frequency. Iron loss was evaluated by using a high frequency iron loss measuring instrument (Metron Inc., type SK-200), and was measured under an excitation magnetic flux density of 1.0 T and frequency of 1 kHz. The difference between iron loss and hysteresis loss was calculated as eddy current loss by Eq. (1).

All the cores after the magnetic measurement were molded so that the cross section in the circumferential direction of the ring was the observation plane, and microstructural observation with an optical microscope was carried out after etching with nital. The crystal grain size was measured by the intercept method²⁷⁾, and the dislocation density was measured by X-ray diffraction by the method proposed by Nakashima et al.²⁸⁾.

3.3 Results and Discussion

3.3.1 Square Ratio of Hysteresis Loop

The results of microstructural observation and magnetic properties of the SMC cores are shown in **Table 2**. In order to separate the contribution of hysteresis loss using the model equation proposed in the previous chapter, it is necessary to determine the square ratio c_h of the hysteresis loop in Eq. (2). The hysteresis loss W_h on the left side of Eq. (2) was obtained by measurement, as shown in Table 2. The measurement conditions of 1.0 T and 1 kHz were substituted for B and f , respectively. H_c and ρ_c were also obtained by measurement, as shown in Table 2. Therefore, c_h is obtained by arranging the relationship between W_h and $(4 \cdot B \cdot f \cdot H_c) / \rho_c$ excluding c_h on the right side of Eq. (2). **Figure 4** shows this relation for all the SMC cores. The plots have a strong linear relationship, and the slope of the trendline gives $c_h = 0.71$. This value is smaller than the c_h obtained in Takajo's previous study because SMC cores were used in this study, while Takajo used a sintered iron core, and it is presumed that the demagnetizing field caused by gaps between iron powder particles affected this value.

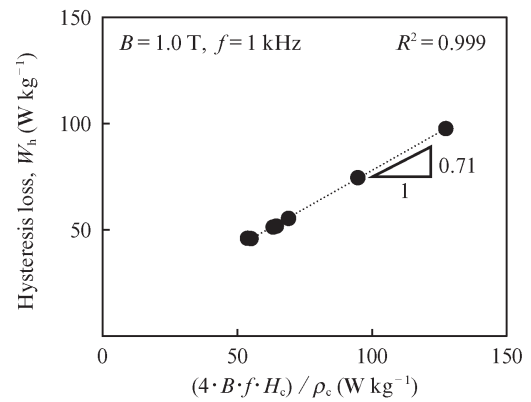


Fig. 4 Relationship between $(4 \cdot B \cdot f \cdot H_c) / \rho_c$ and hysteresis loss

Table 2 Properties of SMC cores

CoreID	Iron loss (1.0 T, 1 kHz) (W kg ⁻¹)		Coercive field, H_c (A m ⁻¹)	Core density, ρ_c (Mg m ⁻³)	Crystal grain size, d_k (μm)	Dislocation density, ρ_d (m ⁻²)
	Hysteresis, W_h	Eddy, W_e				
A-873	46.0	42.1	102.8	7.64	31.3	$3.8 \cdot 10^{12}$
B-873	45.9	31.8	104.9	7.61	27.8	$3.0 \cdot 10^{13}$
B-973	44.8	398.9	105.7	7.64	32.7	$4.2 \cdot 10^{12}$
C-873	51.3	18.5	120.8	7.62	24.1	$1.6 \cdot 10^{12}$
D-673	97.7	7.9	242.9	7.62	25.9	$3.7 \cdot 10^{14}$
D-773	74.6	6.9	181.2	7.64	22.6	$8.2 \cdot 10^{13}$
D-873	55.4	11.2	131.8	7.63	20.3	$2.4 \cdot 10^{12}$
D-973	51.8	545.1	123.6	7.66	22.0	$4.7 \cdot 10^{11}$

3.3.2 Relationship between Crystal Grain Size and Coercive Field

Our previous study⁸⁾ revealed that recrystallization of SMC cores was finished at an annealing temperature of 973 K, and the dislocation density of the annealed core was $1.2 \cdot 10^{-13} \text{ m}^{-2}$. As shown in Table 2, the cores annealed at 873 K had a dislocation density of less than $1.2 \cdot 10^{-13} \text{ m}^{-2}$. Assuming that the contribution of the dislocation density to the coercive force of these cores is on the same level, the coercive force H_c was arranged by the reciprocal of the crystal grain size d_k^{-1} based on the relation in Eq. (2). The result is shown in Fig. 5. The plots have a strong linear relationship, and the slope of the trendline gives $1.7 \cdot 10^3 \text{ A}$, which is in the range of the domain wall energies of pure iron, as shown in Fig. 2. Therefore, Fig. 5 shows the contribution of the crystal grain boundary of the SMC cores, and is expressed experimentally by Eq. (9).

$$H_{c,k} = 1.7 \cdot 10^3 / d_k \dots\dots\dots (9)$$

In the next section, we further discuss the quantification of the contribution of the dislocation density by using Eq. (9).

3.3.3 Relationship between Dislocation Density and Coercive Field

By substituting and arranging Eq. (6) and (9) into Eq. (8), Eq. (10) is obtained.

$$H_c - 1.7 \cdot 10^3 / d_k = \gamma_{\text{dis}} \cdot \rho_d^{1/2} + H_{c,\text{ex}} \dots\dots\dots (10)$$

The left side of Eq. (10) is based on the experimental results. In this study, the $H_{c,\text{ex}}$ of the second term on the right side is considered to be a constant because the chemical compositions of the raw material powders of SMC cores are almost the same. Thus, γ_{dis} is obtained by the relationship between the left side of the equation

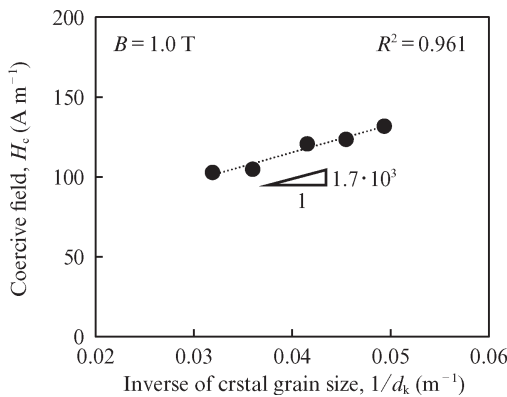


Fig. 5 Relationship between inverse of crystal grain size and $H_{c,k}$

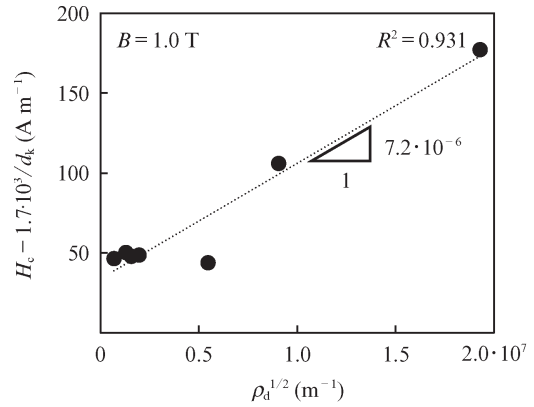


Fig. 6 Relationship between $\rho_d^{1/2}$ and $H_c - 1.7 \cdot 10^3 / d_k$

and $\rho_d^{1/2}$. The result is shown in Fig. 6, and the slope of the trendline gives $\gamma_{\text{dis}} = 7.2 \cdot 10^{-6} \text{ A}$. The analysis is considered to be valid because the γ_{dis} in this study is approximately the same as the γ_{dis} value obtained by Yaegashi²⁴⁾ ($6.5 \cdot 10^{-6} \text{ A}$).

3.3.4 Separation of Contributions by Model Equation

By substituting the values obtained up to the preceding paragraph into Eq. (8), Eq. (11) is obtained.

$$\begin{cases} W_h = W_{h,k} + W_{h,\text{dis}} + W_{h,\text{ex}} \\ \left\{ \begin{aligned} W_{h,k} &= (4 \cdot c_h \cdot B \cdot f) \cdot (1.7 \cdot 10^3) / (d_k \cdot \rho_c) \\ W_{h,\text{dis}} &= (4 \cdot c_h \cdot B \cdot f) \cdot (6.8 \cdot 10^{-6} \cdot \rho_d^{1/2}) / \rho_c \end{aligned} \right. \end{cases} \dots\dots\dots (11)$$

A quantitative analysis of iron loss in relation to the microstructure is possible by using Eq. (1) and (11).

The iron loss analysis result for the SMC cores annealed at 873 K is shown in Fig. 7. The iron loss of D-873 K is the smallest among the cores. Focusing on the loss analysis of D-873, $W_{h,k}$ has the highest ratio. Therefore, to reduce the iron loss of D-873, reduction of $W_{h,k}$ is most important. As can be seen Fig. 7, $W_{h,k}$

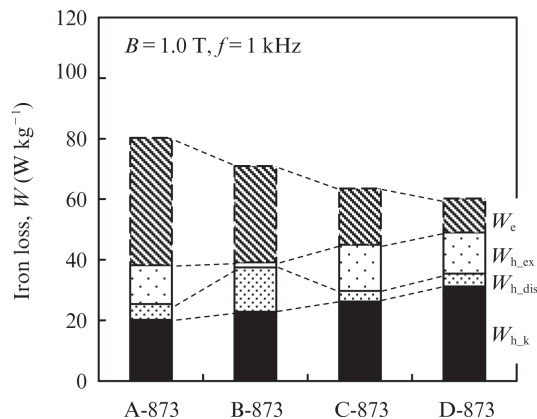


Fig. 7 Effect of raw iron powder particle size on W_e , $W_{h,\text{ex}}$, $W_{h,\text{dis}}$ and $W_{h,k}$

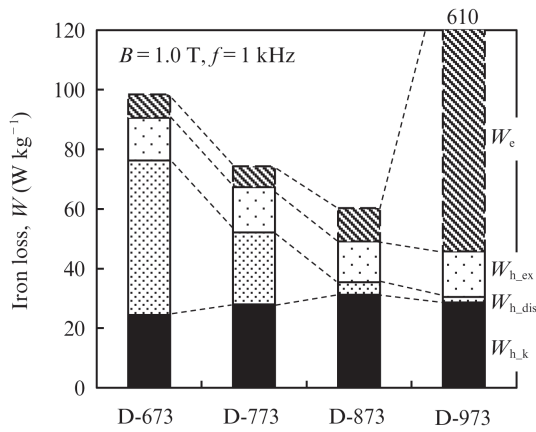


Fig. 8 Effect of raw heat treatment temperature on W_e , $W_{h,ex}$, $W_{h,dis}$ and $W_{h,k}$

decreases with an increase in the raw powder particle size, but because eddy current loss increases with an increase in the raw powder particle size, iron loss increases. From these results, it was found that increasing the raw powder particle size is effective for reducing $W_{h,k}$, but is inappropriate for reducing iron loss.

Next, the iron loss of the SMC cores made from raw iron powder D and its breakdown are shown in Fig. 8. In the range of annealing temperatures from 673 K to 873 K, $W_{h,dis}$ significantly decreases with an increase in the annealing temperature, and as a result, iron loss decreases as the annealing temperature increases. However, $W_{h,k}$ increases with an increase in the annealing temperature. In the range of annealing temperatures from 873 K to 973 K, $W_{h,dis}$ is almost unchanged, and $W_{h,k}$ decreases slightly as the annealing temperature increases. Due to this slight increase of $W_{h,k}$ and the significant decrease of $W_{h,dis}$ with increasing annealing temperature, iron loss decreases as the annealing temperature increases in the range of 673 K to 873 K. However, W_e increases significantly with an increase in the annealing temperature in the range from 873 K to 973 K. Therefore, D-873 has the smallest iron loss in this study.

In addition to the above analysis of iron loss, it is also possible to estimate the theoretical limit value of iron loss of SMC cores by using this model equation. To reduce the iron loss of D-873, crystal grain coarsening is necessary. In SMC cores, the crystal grains cannot be coarsened beyond the particle size of the raw iron powder, so the maximum crystal grain size is determined as $75.6 \mu\text{m}$, which is the average particle size of the powder. The iron loss of D-873 with the maximum crystal grain size was calculated by using Eq. (11) and is shown in Fig. 9. The iron loss is estimated to be 37.3 W kg^{-1} , which is the same as that of electrical steel with a thickness of 0.2 mm. Thus, in theory, there is still ample room for reduction of the iron loss of SMC

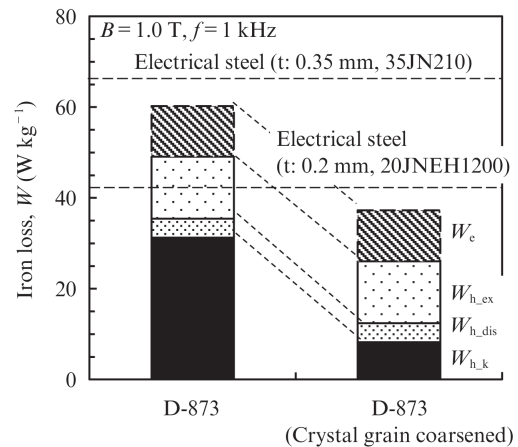


Fig. 9 Possibility of reduction of iron loss of SMC cores by crystal grain coarsened

cores, and lower iron loss can be expected as a result of future progress in material development.

4. Conclusion

In this study, the following knowledge was obtained.

- A quantitative analysis model of hysteresis loss related to microstructural factors of SMC cores was suggested.
- Based on the model, crystal grain coarsening was suggested as a future material development guideline for reducing the iron loss of SMC cores.
- The iron loss of SMC cores estimated by using the model was 37.3 W kg^{-1} , which is the same as that of electrical steel with a thickness of 0.2 mm.

In the future, lower iron loss and expanded application of SMC cores are expected as a result of progress in microstructure control technology for crystal coarsening of SMC cores.

5. Acknowledgment

The authors would like to thank Prof. OZAKI Yukiko of Kyushu University for useful discussions in the course of this research.

Reference

- 1) Sugiyama, M.; Yamaguchi, T.; Okouchi, T.; Kishimoto, S.; Hattori, T.; Saito, T. SOKEIZAI. 2010, no. 51, p. 24–29.
- 2) Saitoh, T.; Enokizono, Y.; Azuma, D.; Ishimine, T.; Ueno, T.; Nakamura, Y.; Okuno, R. SEI Tech. Rev. 2021, no. 198, p. 41–46.
- 3) Kato, T. “Gijyutuskanotamenojiki jiseizairyou.” Nikkankougyou-shinbun, 1991, p. 67.
- 4) Takashita, T. “Gekkan kogyozairyō”. 2021, vol. 69, no. 1, p. 33–37.
- 5) Hojo, H.; Akagi, H.; Sawayama, T.; Mitani, H. Powder for Dust Core with Low Iron Loss. “R&D” Kobe Steel Engineering Reports. 2010, vol. 60, no. 2, p. 79–83.
- 6) Maeda, T.; Sato, A.; Mochida, Y.; Toyoda, H.; Mimura, K.; Nishioka, T. Proc. Powder Metallurgy World Congress. 2006,

- p. 1284–1285.
- 7) Takajo, S. Doctoral dissertation. 1987, Tohoku University.
 - 8) Takashita, T.; Nakamura, N. J. Jpn. Soc. Powder Metallurgy. 2017, vol. 64, no. 8, p. 428–435.
 - 9) Takashita, T.; Ozaki, Y. J. Jpn. Soc. Powder Metallurgy. 2021, vol. 68, no. 1, p. 20–27.
 - 10) Takashita, T.; Ozaki, Y. J. Magn. Magn. Mater. 2021, vol. 535, p. 167992.
 - 11) Takashita, T. Doctoral dissertation. 2021, Kyushu University.
 - 12) A. Mager, *Annalen der physic.* 1952, vol. 6, p. 15–16.
 - 13) T. D. Yensen; N. A. Ziegler. *Trans. Amer. Soc. Met.* 1935, vol. 23, p. 556–557.
 - 14) W. Döring. *Z. Physik.* 1938, vol. 108, p. 137.
 - 15) F. Pfeifer; C. Radloff. *J. of Magn. Magn. Mater.* 1980, vol. 19, p. 190–207.
 - 16) G. Herzer. *IEEE Trans. Magn.* 1990, vol. 26, pp. 1397–1402.
 - 17) R. H. Yu; S. Basu; Y. Zhang; A. Parvizi-Majidi; John Q. Xiao. *J. App. Phys.* 1999, vol. 85, p. 6655–6659.
 - 18) Ohta, K. “*Jikikougakunokiso 2*,” Kyoritsushuppan, 1973, p. 272–273.
 - 19) R. M. Bozorth. *Ferromagnetism*, D. Van Nostrand Company, 1951, p. 54.
 - 20) Chikazumi, S. “*Kyojiseitainobutsuri Vol. 2.*” Shokabo, 1984, p. 175.
 - 21) Chikazumi, S. “*Kyojiseitainobutsuri Vol. 2.*” Shokabo, 1984, p. 4.
 - 22) H. Kronmüller; M. Fähnle. *Micromagnetism and the Microstructure of Ferromagnetic Solids*. Cambridge University Press, 2003, p. 450.
 - 23) H. Träuble. *Magnetism and Metallurgy*. Acad. Press, 1969, p. 621.
 - 24) Yaegashi, H. *Tetsu-to-Hagané*. 2005, vol. 91, p. 655–661.
 - 25) F. Pfeifer; W. Kunz. *J. Magn. Magn. Mat.* 1977, vol. 4, p. 214–219.
 - 26) E. Adler; H. Pfeiffer. *IEEE Trans. Magnetism*. 1974, vol. 10, p. 172–174.
 - 27) Makishima, K. “*Keiryokeitaigaku.*” Uchidarokakuho, 1972, p. 282.
 - 28) Nakashima, K.; Nimura, Y.; Tobitaka, H.; Tsuchiyama, T. Takaki, S. *CAMP-ISIJ*. 2004, vol. 17, p. 396–399.